Struct Multidisc Optim 24, 418–429 © Springer-Verlag 2003
Digital Object Identifier (DOI) 10.1007/s00158-002-0255-6

Numerical method for shape optimization using meshfree method

N.H. Kim, K.K. Choi and M.E. Botkin

Abstract A numerical method for continuum-based shape design sensitivity analysis and optimization using the meshfree method is proposed. The reproducing kernel particle method is used for domain discretization in conjunction with the Gauss integration method. Special features of the meshfree method from a sensitivity analysis viewpoint are discussed, including the treatment of essential boundary conditions, and the dependence of the shape function on the design variation. It is shown that the mesh distortion that exists in the finite element–based design approach is effectively resolved for large shape changing design problems through 2-D and 3-D numerical examples. The number of design iterations is reduced because of the accurate sensitivity information.

Key words design sensitivity analysis, shape optimization, meshfree method, reproducing kernel particle method

1 Introduction

Major computational challenges involved in structural shape optimization using finite element methods (FEM) arise from the excessive mesh distortion that occurs during large shape design changes and mesh–dependent solution accuracy. Numerous difficulties are encountered in finite element analysis, such as those involving mesh distortion, mesh adaptivity, and potentially a large number of re-meshes that are required during the optimization process (Bennett and Botkin 1985; Yao and Choi 1989). Meshfree methods have been proposed to overcome the aforementioned difficulties, in which the shape function is independent of the mesh geometry. The meshfree method is unique because it generates new interpolation/shape functions, which allow field variables to be interpolated at a global level, therefore avoiding the use of mesh. In this paper, a numerical method of shape design sensitivity analysis (DSA), developed in the continuum setting (Choi and Haug 1983), is proposed using the meshfree method. The main purpose of this paper is to introduce special features of the meshfree method from a DSA and optimization viewpoint and its numerical implementation. In addition, mesh distortion and re-meshing problems encountered in FEM–based shape optimization can be avoided and the design costs can be significantly reduced as a result of the accurate and efficient computation of design sensitivity information.

Significant efforts to generate a shape function of interpolation that is independent of mesh geometry have resulted in several meshfree methods. The moving least square method (Lancaster and Salkauskas 1981), the smooth particle hydrodynamics method (Randles and Libersky 1996), the diffuse element method (Nayroles *et al.* 1992), the element free Galerkin method (Belytschko *et al.* 1994), the reproducing kernel particle method (RKPM) (Liu *et al.* 1995), the partition of unity method (PUM) (Melenk and Babuska 1996), and the hp–cloud method (Duarte and Oden 1996) are a short list of meshfree developments. RKPM was further extended to highly nonlinear hyperelastic and elastoplastic problems by Chen *et al.* (1996). RKPM is utilized as an analysis tool in this paper.

For the gradient–based optimization algorithm, an accurate computation of sensitivity information plays a critical role in the convergence rate of the optimization algorithm. Efficient and accurate sensitivity computation, with respect to shape design parameters, can substantially reduce the design optimization costs. Much research has been proposed in the field of DSA for linear problems such as: the discrete method (Adelman and

Received September 3, 2001
Revised manuscript recevied November 26, 2001

N.H. Kim[1], K.K. Choi[2] and M.E. Botkin[3]

[1] Department of Mechanical Engineering, The University of Florida, Gainesville, FL 32611, USA
e-mail: nkim@ccad.uiowa.edu
[2] Center for Computer-Aided Design, The University of Iowa, Iowa City, IA 52242, USA
e-mail: kkchoi@ccad.uiowa.edu
[3] Vehicle Analysis & Dynamics General Motors R&D and Planning, Mail Code 480-106-256, 30500 Mound Rd. 106, Box 9055, Warren, MI 48090-9055, USA
e-mail: mark_e._botkin@gmr.com

Haftka 1986), the material derivative method (Dems and Mroz 1984; Choi and Haug 1983; Belegundu and Rajan 1988; Arora and Cardoso 1992), and the control volume method (Haber 1987; Tortorelli and Wang 1993). Although DSA research has been conducted using a meshfree method in the continuum approach (Grindeanu *et al.* 1998; Kim *et al.* 2000a,b,2001), the meshfree discretization of the design sensitivity equation, which is much different from FEM, has not been presented before. Thus, the numerical method of meshfree DSA needs to be carefully considered, which is the main purpose of this paper. The linear elastic problems are selected in this paper, since the complicated kinematics of the nonlinear problem can divert the reader's attention from the focus of the paper.

The FE shape function depends on the reference geometry of the finite element, which is fixed throughout the design variation, such that only the spatial derivatives of shape function rely on the shape design variation. The shape function of RKPM, however, depends on a global coordinate of material points that are the design parameters for shape DSA. Thus, the design derivative of the shape function, which explicitly depends on design velocity, has to be considered during the implementation of DSA. Since the shape function of RKPM is constructed from the reproducing condition, the material derivative of the reproducing condition is consistently taken in order to obtain the design variation of the meshfree shape function.

The composition of this paper is as follows. In Sect. 2, a brief review of the meshfree method (RKPM) is presented. In Sect. 3, the design sensitivity equation is approximated from the continuum equation. Conditions for the special treatment of the meshfree method in DSA are explained in detail. The mesh distortion problem and the re-meshing procedure, which appear in the FEM-based approach (Bennett and Botkin 1985), are completely resolved for a large shape-changing design problem, as shown in Sect. 4.

2
Review of the meshfree approximation

The theory of the meshfree method has been recently developed in order to remove or reduce a dependency on mesh geometry in the conventional FEM. Insensitiveness to the mesh shape is a very important feature in shape optimization. In addition, a higher accuracy is achieved simply by adding more particles to the structure, but without remodelling the total structure. However, the difficulty in imposing the essential boundary condition, and the relatively high analysis costs remains weaknesses despite the previously mentioned advantages. For the numerical method of DSA, a meshfree method will be described here, even though a detailed description can be found in the papers by Liu *et al.* (1995) and Chen *et al.* (1996).

2.1
Reproducing kernel approximation

Reproducing kernel approximation regularizes the displacement $z(x)$, using the kernel function and the correction function. The kernel function controls the smoothness of the approximation and the correction function contributes to the exact reproduction of polynomials. For given domain $\Omega \in R^1$, displacement is approximated as

$$z^R(x) = \int_{\Omega} C(x;\xi - x)\,\phi_a(\xi - x)\,z(\xi)\,\mathrm{d}\xi\,, \tag{1}$$

where $z^R(x)$ is the reproduced (approximated) displacement of $z(x)$, $C(x;\xi - x)$ is the correction function, and $\phi_a(\xi - x)$ is the kernel function. Suppose that the domain Ω is discretized by a set of particles $[x^1, \ldots, x^I, \ldots, x^{NP}]$, where x^I is the location of particle I, and NP is the total number of particles. Using a simple trapezoidal rule, (1) is discretized into

$$z^R(x) = \sum_{I=1}^{NP} C(x;x^I - x)\phi_a(x^I - x)z^I \Delta x^I\,, \tag{2}$$

where $z^I = z(x^I)$ and Δx^I is a measure of the length (or weight) associated with particle I. It is difficult to determine the value of Δx^I in a multidimensional case, but it can also be treated as a weight of the nodal value. However, in practice the effect of Δx^I will be counterbalanced, as will later be explained.

In this paper, a cubic spline curve is utilized for the kernel function that has a C^2–continuous property. In the case of one–dimensional problem, if $s = \left|(x^I - x)/a\right|$ is the normalized length between point x and surrounding particle point x^I with the support size a, then the kernel function is defined as

$$\phi_a(s) = \frac{1}{6a}\begin{cases} (3s^3 - 6s^2 + 4), & 0 \le s \le 1 \\ -(s-2)^3, & 1 \le s \le 2 \\ 0, & \text{otherwise} \end{cases} \tag{3}$$

which covers length $2a$. In a multi–dimensional case, the products of (3) in each coordinate direction are used. For example, in a three–dimensional case,

$$\phi_{\mathbf{a}}(\mathbf{s}^I) = \phi_{a_x}(s_x^I)\phi_{a_y}(s_y^I)\phi_{a_z}(s_z^I)\,. \tag{4}$$

Each particle $\mathbf{x}^I$ has a support size $\mathbf{a} = [a_x, a_y, a_z]$. In the following derivations, $\mathbf{x} = [x, y, z]^T = [x_1, x_2, x_3]^T$ will be used whenever convenient. Let IP be the number of particles whose support $\mathbf{a}$ covers $\mathbf{x}$. Then, the reproducing kernel approximation of displacement $\mathbf{z}(\mathbf{x})$ in R^3 is

$$\mathbf{z}^R(\mathbf{x}) = \sum_{I=1}^{IP} C\left(\mathbf{x};\mathbf{x}^I - \mathbf{x}\right)\phi_{\mathbf{a}}\left(\mathbf{x}^I - \mathbf{x}\right)\mathbf{z}^I \Delta \mathbf{x}^I\,. \tag{5}$$

The correction function $C(\mathbf{x};\mathbf{x}^I-\mathbf{x})$ can be computed from the linear combination of monomial bases, as

$$C\left(\mathbf{x};\mathbf{x}^I-\mathbf{x}\right)=\mathbf{q}(\mathbf{x})^T\mathbf{H}(\mathbf{x}^I-\mathbf{x})\,, \tag{6}$$

where

$$\mathbf{H}\left(\mathbf{x}^I-\mathbf{x}\right)=\left[1,x^I-x,y^I-y,z^I-z\right]^T, \tag{7}$$

$$\mathbf{q}(\mathbf{x})=[q_0(\mathbf{x}),q_1(\mathbf{x}),q_2(\mathbf{x}),q_3(\mathbf{x})]^T \tag{8}$$

are the basis and coefficient vectors, respectively. $\mathbf{q}(\mathbf{x})$ is computed from the first–order reproducing (or completeness) condition where the approximation in (5) is exact for polynomials up to the order one, i.e. constant and linear functions. After taking a Taylor series expansion of $\mathbf{z}(\mathbf{x})$ and imposing the completeness condition, the following linear system of equations is obtained:

$$\mathbf{M}(\mathbf{x})\,\mathbf{q}(\mathbf{x})=\mathbf{H}(0)\,, \tag{9}$$

where $\mathbf{M}(\mathbf{x})$ is the moment matrix, defined as

$$M_{ij}(\mathbf{x})=\sum_{I=1}^{IP}\phi_{\mathbf{a}}(\mathbf{s}^I)H_i(\mathbf{x}^I-\mathbf{x})H_j\left(\mathbf{x}^I-\mathbf{x}\right). \tag{10}$$

In computing $\mathbf{M}(\mathbf{x})$, the same integration method as in (2) is used, so that the effect of the integration weight is counterbalanced since $\mathbf{q}(\mathbf{x})$ in (9) has the information of $\mathbf{M}(\mathbf{x})^{-1}$.

To develop a shape function for discrete approximation, the correction function in (6) is substituted into the reproducing approximation in (5) as

$$\mathbf{z}^R(\mathbf{x})=\sum_{I=1}^{IP}\mathbf{q}(\mathbf{x})^T\mathbf{H}(\mathbf{x}^I-\mathbf{x})\phi_{\mathbf{a}}(\mathbf{x}^I-\mathbf{x})\mathbf{d}^I\equiv$$
$$\sum_{I=1}^{IP}\Phi^I(\mathbf{x})\mathbf{d}^I\,, \tag{11}$$

where $\mathbf{d}^I$ is the *generalized displacement* of particle I. The function $\Phi^I(\mathbf{x})$ is interpreted as the *meshfree shape function* of particle I, and $\mathbf{d}^I$ is the associated coefficient. The shape function $\Phi^I(\mathbf{x}^J)$ depends on the current coordinate $\mathbf{x}^J$, whereas the FEM shape function only depends on coordinates of the reference geometry. It should also be noted that, in general, the shape function does not bear Kronecker delta properties, i.e. $\Phi^I(\mathbf{x}^J)\neq\delta_{IJ}$. Therefore, for a general function $\mathbf{z}(\mathbf{x})$ which is not a polynomial, $\mathbf{d}^I$ in (11) is not the nodal value of $\mathbf{z}(\mathbf{x}^I)$.

The structural domain is discretized by using non–overlapping integration zone $\Omega=\Omega^1\cup\ldots\cup\Omega^N$, and the standard Gauss integration method is used to evaluate the domain integral (Fig. 1, Chen *et al.* 1996). This domain partitioning is independent of the particle locations, and particles are not interconnected by elements. Figure 1 shows 5×5 integration points (marked by $\times$) in integration zone Ω_X^I. For example, the support size of three particles (I, J, and K) covers the integration point A. Thus, these three particles are used to construct the shape function at point A.

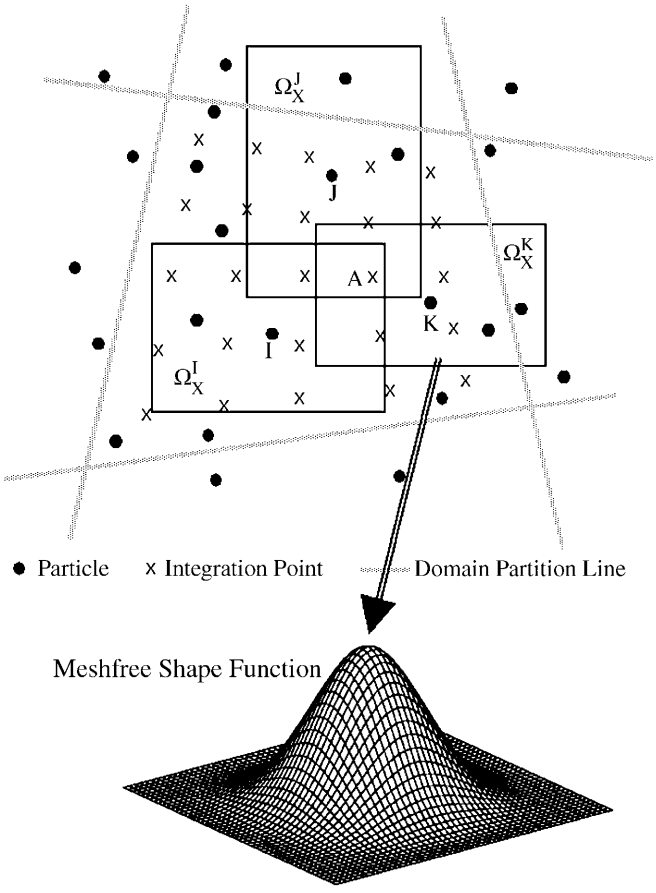

Fig. 1 Domain discretization and meshfree shape function

2.2 Spatial derivatives of the shape function

In FEM, the shape function depends on the reference geometry and its derivative is computed by using a mapping relation between the reference and physical domains. However, the meshfree shape function in (11) depends on the global coordinates of material points, and there is no reference domain. Differentiation of the shape function in (11) is required in structural analysis in order to evaluate stress and strain. From (11), we can obtain

$$\frac{\mathrm{d}\mathbf{z}}{\mathrm{d}x_i}=\sum_{I=1}^{IP}\frac{\mathrm{d}\Phi^I(\mathbf{x})}{\mathrm{d}x_i}\mathbf{d}^I\,, \tag{12}$$

where $\mathrm{d}\Phi^I(\mathbf{x})/\mathrm{d}x_i$ can be calculated from the differential versions of (6) and (9) as

$$\frac{\mathrm{d}\mathbf{q}(\mathbf{x})}{\mathrm{d}x_i}=-\mathbf{M}(\mathbf{x})^{-1}\frac{\mathrm{d}\mathbf{M}(\mathbf{x})}{\mathrm{d}x_i}\mathbf{q}(\mathbf{x})\,, \tag{13}$$

$$\frac{\mathrm{d}C(\mathbf{x};\mathbf{x}^I-\mathbf{x})}{\mathrm{d}x_i}=\frac{\mathrm{d}\mathbf{q}(\mathbf{x})}{\mathrm{d}x_i}^T\mathbf{H}\left(\mathbf{x}^I-\mathbf{x}\right)+$$

$$\mathbf{q}(\mathbf{x})^T\frac{\mathrm{d}\mathbf{H}\left(\mathbf{x}^I-\mathbf{x}\right)}{\mathrm{d}x_i}\,. \tag{14}$$

The expression of $\mathrm{d}\mathbf{M}/\,\mathrm{d}x_i$ and $\mathrm{d}\mathbf{H}/\,\mathrm{d}x_i$ can be obtained from their definitions in (10) and (7), respectively. Thus, the derivative of the shape function can be computed from the derivative of the kernel function, as

$$\frac{\mathrm{d}\Phi^I(\mathbf{x})}{\mathrm{d}x_i}=\frac{\mathrm{d}C\left(\mathbf{x};\mathbf{x}^I-\mathbf{x}\right)}{\mathrm{d}x_i}\phi_{\mathbf{a}}(\mathbf{x}^I-\mathbf{x})+$$

$$C\left(\mathbf{x};\mathbf{x}^I-\mathbf{x}\right)\frac{\mathrm{d}\phi_{\mathbf{a}}(\mathbf{x}^I-\mathbf{x})}{\mathrm{d}x_i}\,. \tag{15}$$

and strain can similarly be computed from (12).

2.3 Variational formulation and meshfree discretization

Let the displacement variation be $\bar{\mathbf{z}}$ and let Z be the space of kinematically admissible displacements that satisfy homogeneous, essential boundary conditions. For given body force f_i^b and the surface traction force f_i^s on the boundary Γ^s, the variational equation in the continuum domain Ω is formulated as

$$a(\mathbf{z},\bar{\mathbf{z}})\equiv\int_\Omega\sigma_{ij}\varepsilon_{ij}(\bar{\mathbf{z}})\,\mathrm{d}\Omega=\int_\Omega\bar{z}_i f_i^b\,\mathrm{d}\Omega+$$

$$\int_{\Gamma^s}\bar{z}_i f_i^s\,\mathrm{d}\Gamma\equiv\ell(\bar{\mathbf{z}})\,, \tag{16}$$

for all $\bar{\mathbf{z}}\in Z$, where σ_{ij} is the stress tensor and ε_{ij} is the engineering strain tensor. In this paper, the superposed "–" denotes the variation of a quantity. For notational convenience, the forms $a\,(\mathbf{z},\bar{\mathbf{z}})$ and $\ell(\bar{\mathbf{z}})$ are used for structural energy and external load, respectively. For linear elastic materials, the constitutive relation is given as

$$\sigma_{ij}(\mathbf{z})=c_{ijk\ell}\varepsilon_{k\ell}(\mathbf{z})\,, \tag{17}$$

where $c_{ijk\ell}$ is the 4^{th}–order stiffness tensor.

The meshfree approximation of (16) in R^2 is derived as follows. From a computational viewpoint, vector notation is simpler than tensor notation, and will therefore be used. The strain tensor $\varepsilon_{ij}(\bar{\mathbf{z}})$ is approximated using the variation of the generalized displacement, as

$$\boldsymbol{\varepsilon}(\bar{\mathbf{d}})=\begin{bmatrix}\varepsilon_{11}(\bar{\mathbf{d}})\\ 2\varepsilon_{12}(\bar{\mathbf{d}})\\ \varepsilon_{22}(\bar{\mathbf{d}})\end{bmatrix}=\sum_{I=1}^{IP}\mathbf{B}_I\bar{\mathbf{d}}^I\,, \tag{18}$$

where $\bar{\mathbf{d}}^I=[\bar{d}_1^I\ \bar{d}_2^I]^T$ is the variation of generalized displacement at the particle point $\mathbf{x}^I$, and $\mathbf{B}_I$ is the strain–displacement matrix, defined as

$$\mathbf{B}_I=\begin{bmatrix}\Phi^I_{,1} & \Phi^I_{,2} & 0\\ 0 & \Phi^I_{,1} & \Phi^I_{,2}\end{bmatrix}^T\,. \tag{19}$$

The subscribed comma represents the spatial derivative, i.e., $\Phi^I_{,j}=\partial\Phi^I/\partial x_j$, whose expression is given in (15). The stress vector is defined for a two–dimensional domain as

$$\boldsymbol{\sigma}=\begin{bmatrix}\sigma_{11}\\ \sigma_{12}\\ \sigma_{22}\end{bmatrix}=\mathbf{C}\,\boldsymbol{\varepsilon}(\mathbf{d})\,, \tag{20}$$

where $\mathbf{C}$ is the stiffness matrix corresponding to $c_{ijk\ell}$ in (17), and $\boldsymbol{\varepsilon}(\mathbf{d})$ has the same expression as (18) if generalized displacement $\mathbf{d}$ is used instead of $\bar{\mathbf{d}}$.

Let the structural domain be partitioned with an N number of integration zones and let the traction boundary be composed of an M number of integration zones. The approximation of $a\,(\mathbf{z},\bar{\mathbf{z}})$ and $\ell(\bar{\mathbf{z}})$ can be expressed in terms of the global generalized displacement vector $\mathbf{d}=[\mathbf{d}^1,\mathbf{d}^2,\ldots,\mathbf{d}^{NP}]^T$, and along with its variations, as

$$a\,(\mathbf{z},\bar{\mathbf{z}})\approx\sum_{i=1}^{N}\int_{\Omega^i}\sum_{I=1}^{IP}\sum_{J=1}^{JP}\bar{\mathbf{d}}^{I^T}\mathbf{B}_I^T\mathbf{C}\mathbf{B}_J\mathbf{d}^J\,\mathrm{d}\Omega\equiv$$

$$\bar{\mathbf{d}}^T\mathbf{K}\,\mathbf{d}\,, \tag{21}$$

$$\ell(\bar{\mathbf{z}})\approx\sum_{i=1}^{N}\int_{\Omega^i}\sum_{I=1}^{IP}\Phi^I\bar{\mathbf{d}}^{I^T}\mathbf{f}^b\,\mathrm{d}\Omega+$$

$$\sum_{i=1}^{M}\int_{\Gamma^i}\sum_{I=1}^{IP}\Phi^I\bar{\mathbf{d}}^{I^T}\mathbf{f}^s\,\mathrm{d}\Omega\equiv\bar{\mathbf{d}}^T\mathbf{F}\,. \tag{22}$$

Using (21) and (22), the discretized variational equation of (16) is obtained as

$$\bar{\mathbf{d}}^T\mathbf{K}\,\mathbf{d}=\bar{\mathbf{d}}^T\mathbf{F}\,, \tag{23}$$

for all $\bar{\mathbf{d}}$ whose counterparts $\bar{\mathbf{z}}$ belong to Z.

Since it is difficult to make $\bar{\mathbf{d}}$ belong to Z, a transformation has to be used in order to construct an admissible displacement space. There are several ways to construct an admissible displacement variation (Chen *et al.* 2000a). In this paper, the full transformation and mixed transformation methods are explained. Since the space of kinematically admissible displacements cannot be easily chosen from the generalized displacement, the generalized displacement variation in (23) is transformed into the physical displacement variation, using the following relation:

$$\mathbf{z}^J=\mathbf{z}(\mathbf{x}^J)=\sum_{I=1}^{IP}\Phi^I(\mathbf{X}^J)\mathbf{d}^I\equiv\sum_{I=1}^{IP}A_{IJ}\mathbf{d}^I\,,$$

$$\mathbf{z}_g=\mathbf{A}^T\mathbf{d}\,, \tag{24}$$

where $\mathbf{A}$ is the matrix that transforms the generalized displacement into the physical displacement and $\mathbf{z}_g = [\mathbf{z}^1, \mathbf{z}^2, \ldots, \mathbf{z}^{NP}]^T$ denotes the global displacement vector of the discretized domain. The variations of displacements have a similar relation as (24). By imposing an inverse relation of (24) onto (23) for $\bar{\mathbf{d}}$,

$$\bar{\mathbf{z}}_g^T \mathbf{A}^{-1} \mathbf{K}\, \mathbf{d} = \bar{\mathbf{z}}_g^T \mathbf{A}^{-1} \mathbf{F}, \quad \forall \bar{\mathbf{z}}_g \in Z_g\,, \tag{25}$$

where Z_g is the space of kinematically admissible displacements in the discretized domain. By defining $\mathbf{K}^* = \mathbf{A}^{-1}\mathbf{K}$ and $\mathbf{F}^* = \mathbf{A}^{-1}\mathbf{F}$, the following linear matrix equation is solved:

$$\mathbf{K}^* \mathbf{d} = \mathbf{F}^*\,. \tag{26}$$

Note that $\mathbf{K}^*$ is indefinite because of rigid body motion. For the displacement boundary condition, let the displacement of the particle J be prescribed as $\mathbf{z}^J = \mathbf{g}^J$. The essential boundary condition is imposed using the relation established in (24), as

$$\sum_{I=1}^{IP} A_{IJ} \mathbf{d}^I = \mathbf{g}^J\,. \tag{27}$$

This relation is substituted into (26) for the corresponding degree–of–freedom location of the essential boundary condition, which makes $\mathbf{K}^*$ positive definite. After solving for the generalized displacement $\mathbf{d}$, the physical displacement can be calculated from (24).

The expensive computational cost of the meshfree method comes from the following three factors: (1) the number of particles during the meshfree approximation in (11) is usually greater than that of FEM, (2) the domain integration requires large number of integration points as shown in Fig. 1 because the shape function is higher order than that of FEM, and (3) the calculation of $\mathbf{A}^{-1}$ in (25) is more expensive than solving the matrix equation (26). The first two properties are not significant disadvantages since the approximation that is more accurate is obtained because of them.

In order to reduce the computation cost involved in (25), the mixed transformation method (Chen *et al.* 2000a) is used in this paper. Since the purpose of (25) is to construct kinematically admissible displacements, it is necessary to transform only those particles that belong to the essential boundary. Thus, a new discrete vector $\hat{\bar{\mathbf{d}}}$ is defined from $\bar{\mathbf{d}}$ as

$$\hat{\bar{\mathbf{d}}} \equiv \begin{Bmatrix} \bar{\mathbf{z}}_B \\ \bar{\mathbf{d}}_I \end{Bmatrix} = \begin{bmatrix} \mathbf{a}_{BB} & \mathbf{a}_{BI} \\ \mathbf{0} & \mathbf{I} \end{bmatrix} \begin{Bmatrix} \bar{\mathbf{d}}_B \\ \bar{\mathbf{d}}_I \end{Bmatrix} \equiv \mathbf{\Lambda}\, \bar{\mathbf{d}}\,, \tag{28}$$

where the subscribed B represents the essential boundary nodes, while I denotes interior nodes. The component matrix of $\mathbf{\Lambda}$ is obtained from the component matrix of $\mathbf{A}$ as

$$\mathbf{A} = \begin{bmatrix} \mathbf{a}_{BB} & \mathbf{a}_{BI} \\ \mathbf{a}_{IB} & \mathbf{a}_{II} \end{bmatrix}. \tag{29}$$

Instead of the matrix $\mathbf{A}$, the matrix $\mathbf{\Lambda}$ can be used for the transformation in (25). The computational advantage of using the matrix $\mathbf{\Lambda}$ is that the inverse matrix $\mathbf{\Lambda}^{-1}$ can be calculated much easier than $\mathbf{A}^{-1}$. That is,

$$\mathbf{\Lambda}^{-1} = \begin{bmatrix} \mathbf{a}_{BB}^{-1} & -\mathbf{a}_{BB}^{-1}\mathbf{a}_{BI} \\ \mathbf{0} & \mathbf{I} \end{bmatrix}. \tag{30}$$

In fact, it is unnecessary to store the whole matrix $\mathbf{\Lambda}$. The small component matrices $\mathbf{a}_{BB}$ and $\mathbf{a}_{BI}$ need to be stored, which is much smaller in size than the matrix $\mathbf{a}_{II}$.

3 Shape design sensitivity analysis

3.1 Material derivative and design sensitivity equation

In shape design, the shape of the domain that a structural component occupies is treated as a design variable. Suppose that the initial structural domain Ω is changed into the perturbed domain Ω_τ in which the parameter τ controls the shape perturbation amount. By defining the design changing direction to be $\mathbf{V}(\mathbf{x})$, the material point at the perturbed design can be denoted as $\mathbf{x}_\tau = \mathbf{x} + \tau \mathbf{V}(\mathbf{x})$. The solution $\mathbf{z}_\tau(\mathbf{x}_\tau)$ of structural problems is assumed a differentiable function with respect to shape design. The material derivative of $\mathbf{z}_\tau(\mathbf{x}_\tau)$ at $\mathbf{x} \in \Omega$ is defined as

$$\dot{\mathbf{z}} = \lim_{\tau \to 0} \frac{\mathbf{z}_\tau\left(\mathbf{x} + \tau \mathbf{V}(\mathbf{x})\right) - \mathbf{z}(\mathbf{x})}{\tau}\,. \tag{31}$$

The design sensitivity equation is obtained by taking the material derivative of the variational equation (16). The derivative of the energy form then becomes

$$\frac{\mathrm{d}}{\mathrm{d}\tau} a_\tau(\mathbf{z}_\tau, \bar{\mathbf{z}}_\tau)\bigg|_{\tau=0} = a\left(\dot{\mathbf{z}}, \bar{\mathbf{z}}\right) + a'_V(\mathbf{z}, \bar{\mathbf{z}})\,. \tag{32}$$

The first term on the right-hand side represents an implicit dependence on design through the state variable, while the second term, the structural fictitious load, denotes an explicit dependence on the design velocity $\mathbf{V}(\mathbf{x})$, defined as

$$a'_V(\mathbf{z}, \bar{\mathbf{z}}) = \int_\Omega \Big[\varepsilon_{ij}^V(\bar{\mathbf{z}})\sigma_{ij}(\mathbf{z}) + \varepsilon_{ij}(\bar{\mathbf{z}}) c_{ijkl} \varepsilon_{kl}^V(\mathbf{z}) + \varepsilon_{ij}(\bar{\mathbf{z}})\sigma_{ij}(\mathbf{z})\, div\mathbf{V}\Big]\, \mathrm{d}\Omega\,, \tag{33}$$

where

$$\varepsilon_{ij}^V(\mathbf{z}) = -\frac{1}{2}\left(\frac{\partial z_i}{\partial x_k}\frac{\partial V_k}{\partial x_j} + \frac{\partial z_j}{\partial x_k}\frac{\partial V_k}{\partial x_i}\right). \tag{34}$$

If the applied load is independent of displacement, i.e. conservative, then the external fictitious load form becomes

$$\ell'_V(\bar{\mathbf{z}}) = \int_\Omega \left[\bar{z}_i \frac{\partial f_i^b}{\partial x_j} V_j + \bar{z}_i f_i^b \frac{\partial V_j}{\partial x_j} \right] \mathrm{d}\Omega +$$

$$\int_{\Gamma^s} \left[\bar{z}_i \frac{\partial f_i^s}{\partial x_j} V_j + \kappa \bar{z}_i f_i^s V_n \right] \mathrm{d}\Gamma \,, \tag{35}$$

where V_n is the normal component of the design velocity on the boundary, and κ is the curvature of the boundary. The design sensitivity equation is obtained from (32) and (35), as

$$a\,(\dot{\mathbf{z}}, \bar{\mathbf{z}}) = \ell'_V(\bar{\mathbf{z}}) - a'_V(\mathbf{z}, \bar{\mathbf{z}}), \qquad \forall \bar{\mathbf{z}} \in Z \,. \tag{36}$$

Note that by substituting $\mathbf{z}$ into $\dot{\mathbf{z}}$, the left of the design sensitivity equation (36) takes the same form as that of the response analysis in (16). Thus, the same stiffness matrix can be used for DSA and response analysis, with a different right-hand side.

After calculating the material derivative of state variable $\dot{\mathbf{z}}$ with respect to the shape design variable, the sensitivity of the general performance measure (cost and constraint function)

$$\psi = \int_\Omega g(z_i, z_{i,j}) \, \mathrm{d}\Omega \tag{37}$$

can be obtained using a chain rule of differentiation, as

$$\psi' = \int_\Omega [g_{,z_i} \dot{z}_i + g_{,z_{i,j}} \dot{z}_{i,j} + g V_{i,i} -$$

$$g_{,z_{i,j}} z_{i,k} V_{k,j}] \, \mathrm{d}\Omega \,. \tag{38}$$

The computation of design sensitivity using (38) is called the *direct differentiation method*; in contrast, the *adjoint variable method* (Choi and Haug 1983) uses an adjoint equation to solve $\dot{\mathbf{z}}$ explicitly in terms of the design velocity field.

3.2 Meshfree discretization of design sensitivity equation

Since the main unknown variable of the meshfree method is generalized displacement $\mathbf{d}$, the design sensitivity equation (36) of a continuum form, which is written in terms of $\dot{\mathbf{z}}$, has to be discretized using $\dot{\mathbf{d}}$. Since displacement $\mathbf{z}$ is approximated using the meshfree shape function in (11), $\dot{\mathbf{z}}$ can be approximated as

$$\dot{\mathbf{z}}^I = \sum_{I=1}^{IP} \left(\Phi^I \dot{\mathbf{d}}^I + \dot{\Phi}^I \mathbf{d}^I \right),$$

$$\dot{\mathbf{z}}_g = \mathbf{A}^T \dot{\mathbf{d}} + \dot{\mathbf{A}}^T \mathbf{d} \,. \tag{39}$$

This decomposition is quite different from FEM in which shape function is independent of design. The first term of (39) constitutes the main unknown $\dot{\mathbf{d}}$ of the design sensitivity equation in meshfree approximation, while the second term represents the dependence of the shape function on design, which is explicit in $\mathbf{V}(\mathbf{x})$. A numerical method to compute $\dot{\Phi}^I(\mathbf{x})$ will now be introduced.

From the relation $\mathbf{x}_\tau = \mathbf{x} + \tau \mathbf{V}(\mathbf{x})$, the derivative of the material point $\mathbf{x}$ with respect to design is nothing but the design velocity $\mathbf{V}(\mathbf{x})$. Consider the material derivative of the kernel function in (3) for a one–dimensional problem,

$$\dot{\phi}_a(s) = \frac{V^I - V}{2a^2} \begin{cases} (3s^2 - 4s), & 0 \le s \le 1 \\ -(s-2)^2, & 1 \le s \le 2 \\ 0, & \text{otherwise} \end{cases} \tag{40}$$

where V^I is the design velocity at x^I, and V is the design velocity at x. For a multi–dimensional problem, the product rule in (4) can be used. To compute $\dot{\Phi}^I(\mathbf{x})$, the design derivative of the reproducing condition has to be taken. By taking the design derivative of the completeness condition in (9), and using (10),

$$\dot{\mathbf{q}} = -\mathbf{M}^{-1} \dot{\mathbf{M}} \, \mathbf{q} \,, \tag{41}$$

$$\dot{M}_{ij} = \sum_{I=1}^{IP} \left[\dot{\phi}_{\mathbf{a}} H_i H_j + \phi_{\mathbf{a}} \dot{H}_i H_j + \phi_{\mathbf{a}} H_i \dot{H}_j \right], \tag{42}$$

$$\dot{\mathbf{H}} = \left[0, V_x^I - V_x, V_y^I - V_y, V_z^I - V_z \right]^T . \tag{43}$$

Thus, from the definition in (11) and from the product rule of differentiation,

$$\dot{\Phi}^I = \dot{\mathbf{q}}^T \mathbf{H} \phi_{\mathbf{a}} + \mathbf{q}^T \dot{\mathbf{H}} \phi_{\mathbf{a}} + \mathbf{q}^T \mathbf{H} \dot{\phi}_{\mathbf{a}} \,. \tag{44}$$

For given design velocity $\mathbf{V}(\mathbf{x})$, (44) can be explicitly calculated even before any sensitivity analysis. The design derivative of $\mathrm{d}\Phi^I(\mathbf{x})/\mathrm{d}\mathbf{x}$ in (15) can also be calculated using a similar procedure as has been described above, but requiring lengthy algebraic calculations.

In a DSA procedure, it is frequently necessary to take the material derivative of a strain tensor or, equivalently, the gradient of displacement $z_{i,j} = \partial z_i / \partial x_j$. Choi and Haug (1983) uses the concept of a partial derivative that is commutable to a spatial gradient. By using (11) and (39), a meshfree approximation of the design derivative of $z_{i,j}$ can be expressed as

$$\frac{\mathrm{d}}{\mathrm{d}\tau}(z_{i,j}) = \sum_{I=1}^{IP} \left(\Phi^I_{,j} \dot{d}_i^I + \dot{\Phi}^I_{,j} d_i^I - \Phi^I_{,k} d_i^I V_{k,j} \right). \tag{45}$$

Note that the last term is used in the construction of $\boldsymbol{\varepsilon}^V$ in (34) and the additional term $\dot{\Phi}^I_{,j} d_i^I$ appears that is explicitly dependent on design velocity. The only unknown is $\dot{d}_i^I$ which will be computed from the design sensitivity

equation. To simplify the approximation of (45), consider the following relation:

$$\frac{\mathrm{d}}{\mathrm{d}\tau}(\Phi^I_{,i}) = \dot{\Phi}^I_{,i} - \Phi^I_{,k} V_{k,i}\,. \tag{46}$$

Thus, the last two terms of (45) can be combined together to represent an explicitly dependent term on $\mathbf{V}(\mathbf{x})$ through $\frac{\mathrm{d}}{\mathrm{d}\tau}(\Phi^I_{,i})$. Using (46), (45) is simplified to

$$\frac{\mathrm{d}}{\mathrm{d}\tau}(z_{i,j}) = \sum_{I=1}^{IP}(\Phi^I_{,j}\dot{d}^I_i) + \sum_{I=1}^{IP}\left[\frac{\mathrm{d}}{\mathrm{d}\tau}(\Phi^I_{,j})d^I_i\right]\,. \tag{47}$$

Note that the two summations of (47) have a similar format. The first term on the right-hand side has to be solved using a design sensitivity equation, and the second term can be computed explicitly in terms of the design velocity $\mathbf{V}(\mathbf{x})$ using relation (44).

In the development of a DSA, it is usually assumed that the space Z is independent of shape design, i.e. $\dot{\bar{\mathbf{z}}} = 0$. However, this assumption may not be true for all situations. Even if the assumption of $\dot{\bar{\mathbf{z}}} = 0$ is not used, since $\dot{\bar{\mathbf{z}}} \in Z$, the following relation is satisfied:

$$a\,(\mathbf{z}, \dot{\bar{\mathbf{z}}}) = \ell(\dot{\bar{\mathbf{z}}})\,. \tag{48}$$

Because of (48), the contribution of $\dot{\bar{\mathbf{z}}}$ in (36) was ignored. In addition, from the relation in (45),

$$\frac{\mathrm{d}}{\mathrm{d}\tau}(\bar{z}_{i,j}) = -\bar{z}_{i,k}V_{k,j} = -\sum_{I=1}^{IP}\Phi^I_{,k}\bar{d}^I_i V_{k,j}\,. \tag{49}$$

An approximation of the design sensitivity equation (36) follows the same method as a response analysis. For a given meshfree shape function, using its material derivatives from (44), as well as using the relation in (47), the following approximation can be obtained:

$$\boldsymbol{\varepsilon}^V(\mathbf{z}) = \sum_{I=1}^{IP}\dot{\mathbf{B}}_I\mathbf{d}^I\,, \tag{50}$$

where $\dot{\mathbf{B}}_I$ is the design derivative of $\mathbf{B}_I$ in (19), defined by

$$\dot{\mathbf{B}}_I = \begin{bmatrix} \frac{\mathrm{d}}{\mathrm{d}\tau}(\Phi^I_{,1}) & \frac{\mathrm{d}}{\mathrm{d}\tau}(\Phi^I_{,2}) & 0 \\ 0 & \frac{\mathrm{d}}{\mathrm{d}\tau}(\Phi^I_{,1}) & \frac{\mathrm{d}}{\mathrm{d}\tau}(\Phi^I_{,2}) \end{bmatrix}^T\,. \tag{51}$$

In contrast, the approximation of $\boldsymbol{\varepsilon}^V(\bar{\mathbf{z}})$ has a different expression because of (49),

$$\boldsymbol{\varepsilon}^V(\bar{\mathbf{z}}) = \sum_{I=1}^{IP}\mathbf{B}^V_I\bar{\mathbf{d}}^I\,, \tag{52}$$

where

$$\mathbf{B}^V_I = -\begin{bmatrix} \Phi^I_{,k}V_{k,1} & \Phi^I_{,k}V_{k,2} & 0 \\ 0 & \Phi^I_{,k}V_{k,1} & \Phi^I_{,k}V_{k,2} \end{bmatrix}^T\,. \tag{53}$$

Thus, the structural fictitious load in (33) and the external fictitious load in (35) are discretized by

$$a'_V(\mathbf{z}, \bar{\mathbf{z}}) \approx \sum_{i=1}^{N}\int_{\Omega^i}\sum_{I=1}^{IP}\bar{\mathbf{d}}^{I^T}\Big[\mathbf{B}_I^{V^T}\boldsymbol{\sigma} + \mathbf{B}_I^T\mathbf{C}\,\boldsymbol{\varepsilon}^V(\mathbf{z}) + \mathbf{B}_I^T\boldsymbol{\sigma}\,div\mathbf{V}\Big]\,\mathrm{d}\Omega \equiv \bar{\mathbf{d}}^T\mathbf{F}^a\,, \tag{54}$$

$$\ell'_V(\bar{\mathbf{z}}) \approx \sum_{i=1}^{N}\int_{\Omega^i}\sum_{I=1}^{IP}\bar{\mathbf{d}}^{I^T}\left[\Phi^I(\nabla\mathbf{f}^b\mathbf{V} + \mathbf{f}^b\,div\mathbf{V})\right]\mathrm{d}\Omega + \sum_{i=1}^{M}\int_{\Gamma^i}\sum_{I=1}^{IP}\bar{\mathbf{d}}^{I^T}\left[\Phi^I(\nabla\mathbf{f}^s\mathbf{V} + \kappa\,\mathbf{f}^s\,V_n)\right]\mathrm{d}\Gamma \equiv \bar{\mathbf{d}}^T\mathbf{F}^\ell\,. \tag{55}$$

The global discretized variational equation of DSA is obtained from (36) as

$$\bar{\mathbf{d}}^T\mathbf{K}\,\dot{\mathbf{d}} = \bar{\mathbf{d}}^T(\mathbf{F}^\ell - \mathbf{F}^a)\,, \tag{56}$$

for all $\bar{\mathbf{d}}$ whose counterparts $\bar{\mathbf{z}}_g$ belong to Z_g. By following the same response analysis procedure to construct kinematically admissible displacements, the following linear matrix equation is solved:

$$\mathbf{K}^*\dot{\mathbf{d}} = \mathbf{A}^{-1}(\mathbf{F}^\ell - \mathbf{F}^a)\,, \tag{57}$$

where $\mathbf{K}^*$ represents the same stiffness matrix of response analysis as in (26), which is already factorized. Thus, it is very efficient to solve (57) with different right sides. If the mixed transformation method is used, then the matrix $\mathbf{\Lambda}^{-1}$ in (30) can be used instead of $\mathbf{A}^{-1}$.

Consideration of the essential boundary conditions is somewhat different from that of the analysis undertaken in (27), since the transformation matrix $\mathbf{A}$, which is composed of a meshfree shape function, depends on the shape design. Let the prescribed displacement $\mathbf{g}^J$ at $\mathbf{x}^J$ be independent of design, which is true in most cases. Then, from the design derivative of (27),

$$\sum_{I=1}^{IP}A_{IJ}\dot{\mathbf{d}}^I = -\sum_{I=1}^{IP}\dot{A}_{IJ}\mathbf{d}^I\,, \tag{58}$$

where $\dot{A}_{IJ} = \dot{\Phi}^I(\mathbf{x}^J)$ is obtained from (39). Equation (58) is substituted into (57) for those rows that correspond to the degree–of–freedom of $\mathbf{x}^J$. Equation (57) is solved for each design parameter with the same decomposed $\mathbf{K}^*$ matrix. After solving $\dot{\mathbf{d}}$, the material derivative of physical displacement can be calculated from the relation in (39). Note that the transformation matrix $\mathbf{A}$ and its material derivative $\dot{\mathbf{A}}$ have the same form for different transformation methods. Thus, the implementation of DSA is independent of transformation method.

4
Numerical examples

4.1
Shape design optimization of a torque arm

This paper uses a torque arm design optimization problem, presented by Bennett and Botkin (1985), as a numerical example. The geometry of the torque arm (see Fig. 2) is modelled using The MacNeal–Schwendler Corp. (1999), and is represented by parametric coordinates. Design parameterization was performed by selecting the control points of the parametric curves. Design velocity vectors that represent the movement of particles in the direction of a given design parameter were computed by perturbing the parametric coordinates. This process is referred to as the isoparametric mapping method. Design parameterization and design velocity vector computation were also carried out by using a *Design Sensitivity and Optimization Tool* (DSO) code (Chang *et al.* 1995), developed by the authors and the co–workers of this article. In all, eight design parameters were chosen in order to perturb the outer/inner boundary curves of the torque arm.

An automatic particle–generation procedure was used to distribute meshfree particles over the structure. The domain of the torque arm was discretized by 239 RKPM particles (478 DOF), as shown in Fig. 2. The plane stress formulation is used with a thickness of 0.3 cm. The torque arm is made of steel with $E = 207$ GPa, and $\nu = 0.3$.

The meshfree analysis required 5.19 sec., whereas by using one processor of HP Exemplar s-class workstation DSA required 0.57 seconds per each design parameter. The efficiency of the sensitivity computation derives from the fact that DSA uses the same stiffness matrix, already factorized from the response analysis stage.

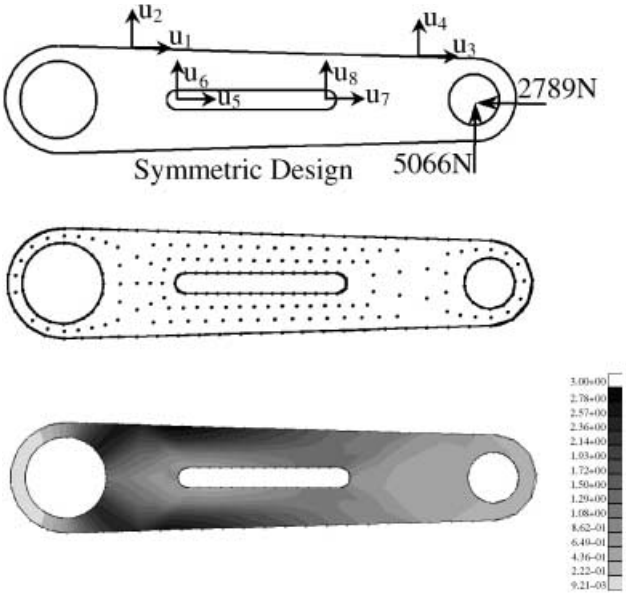

Fig. 2 Design parameterization and meshfree analysis result of torque arm

The sensitivity coefficients of the performance measures, including the structural area and the stresses, were computed based on the continuum approach. The highest stress values at 19 integration zones are selected as performance measure, which will be served as constraints during optimization. Using a very small perturbation size, the accuracy of the sensitivity coefficients is compared with the finite difference method in Table 1. Very accurate sensitivity results are observed. In Table 1, the first column represents design parameters, the second column represents performance measures, i.e. structural area and von Mises stress at eight integration zones. The third column $\Delta\psi$ denotes the first–order sensitivity results obtained from the forward finite difference method with a perturbation of $\tau = 10^{-6}$. The fourth column represents the sensitivity computation results from the method employed. As shown in the last column, the sensitivity results from two methods match quite well.

Table 1 Design sensitivity results and comparison with finite difference results

u	ψ	$\Delta\psi$	ψ'	$\Delta\psi/\psi' \times 100$
	Area	0.10361×10^{-5}	0.10362×10^{-5}	100.00
	σ_{82}	-0.62892×10^{-7}	-0.62891×10^{-7}	100.00
	σ_{85}	-0.17736×10^{-8}	-0.17722×10^{-8}	100.08
	σ_{88}	-0.88829×10^{-7}	-0.88828×10^{-7}	100.00
u_1	σ_{91}	-0.11245×10^{-6}	-0.11245×10^{-6}	100.00
	σ_{97}	-0.77783×10^{-7}	-0.77781×10^{-7}	100.00
	σ_{136}	-0.15990×10^{-6}	-0.15991×10^{-6}	100.00
	σ_{133}	0.33665×10^{-7}	0.33667×10^{-7}	100.00
	σ_{100}	-0.67624×10^{-7}	-0.67623×10^{-7}	100.00
	Area	0.10118×10^{-5}	0.10119×10^{-5}	100.00
	σ_{82}	-0.78084×10^{-9}	-0.78177×10^{-9}	99.88
	σ_{85}	0.14674×10^{-9}	0.14678×10^{-9}	99.97
	σ_{88}	-0.58752×10^{-8}	-0.58748×10^{-8}	100.01
u_3	σ_{91}	-0.19387×10^{-7}	-0.19387×10^{-7}	100.00
	σ_{97}	-0.39358×10^{-7}	-0.39357×10^{-7}	100.00
	σ_{136}	-0.38821×10^{-9}	-0.38886×10^{-9}	99.83
	σ_{133}	0.41596×10^{-9}	0.41525×10^{-9}	100.17
	σ_{100}	-0.59788×10^{-7}	-0.59787×10^{-7}	100.00
	Area	-0.20000×10^{-5}	-0.20000×10^{-5}	100.00
	σ_{82}	0.20682×10^{-8}	0.20709×10^{-8}	99.87
	σ_{85}	0.47302×10^{-8}	0.47324×10^{-8}	99.95
	σ_{88}	0.60386×10^{-8}	0.60409×10^{-8}	99.96
u_7	σ_{91}	0.81475×10^{-8}	0.81496×10^{-8}	99.98
	σ_{97}	0.16225×10^{-7}	0.16227×10^{-7}	99.99
	σ_{136}	-0.78753×10^{-9}	-0.78694×10^{-9}	100.08
	σ_{133}	0.26136×10^{-9}	0.26181×10^{-9}	99.83
	σ_{100}	0.25006×10^{-7}	0.25008×10^{-7}	99.99

The design optimization problem is formulated in such a way that the total area of the structure is minimized with respect to its shape design parameters, with design constraints defined as the second invariant of the stress tensors (von Mises stress), as

$$\begin{array}{ll} \text{minimize} & \text{mass} \\ \text{subject to} & \sigma_{\text{MAX}} \leq 800\,\text{MPa}\,' \end{array} \tag{59}$$

The sequential quadratic programming method has been used in a commercially–available optimization program (Vanderplaats 1997). Figure 3 shows the meshfree analysis results at optimum design where the stress constraints along the upper side of torque arm became active. No remodelling was used during the design optimization procedure.

Figure 4 provides an optimization history of the cost function. Through optimization, the structural mass was reduced from 0.878 kg to 0.421 kg (47.9%). The highest stress value initially, 305 MPa around the left hole, shifts to 800 MPa around the upper frame at optimum design. A total of 41 response analyses and 20 DSA were carried out during 20 optimization iterations. When FEA is used with a re-meshing process (Bennett and Botkin 1985), the optimization process converged at 45 iterations with eight re-meshing processes. Thus, this approach reduces the cost of design more than 50%, without even mentioning the cost related to the re-meshing process.

Since the initial particle distribution was used throughout the design optimization process, a very irregular particle distribution resulted in the optimum design. To confirm the accuracy of the analysis, remodelling was carried out in order to redistribute particles evenly at the optimum design stage. Figure 5 shows that the analysis results for the redistributed meshfree particles are very similar to the results from the irregular distribution in Fig. 3. Thus, it is clear that particle distortion does not significantly contribute to either the solution accuracy or the optimum result.

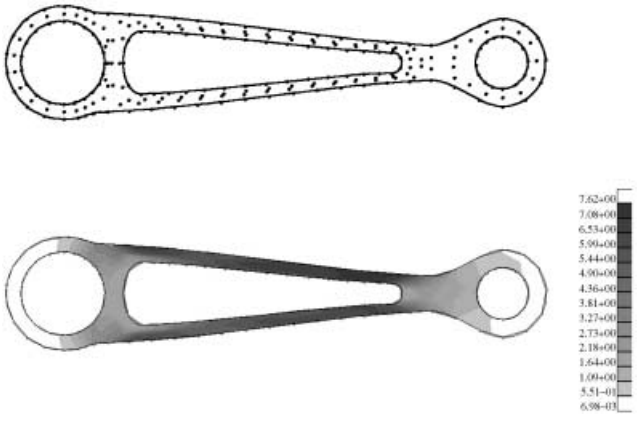

Fig. 3 Analysis result at optimum design

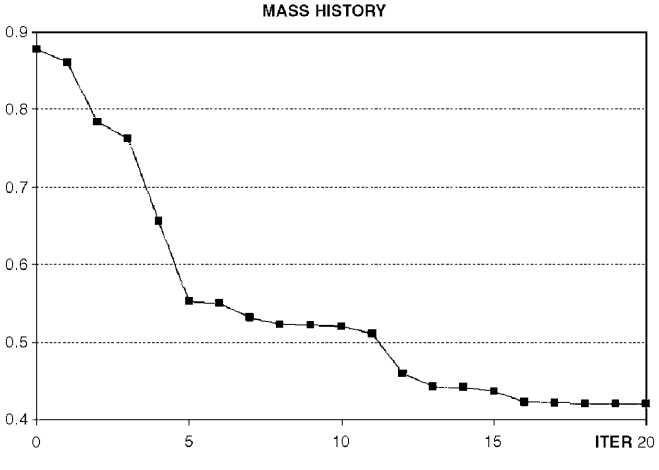

Fig. 4 Histories of design optimization

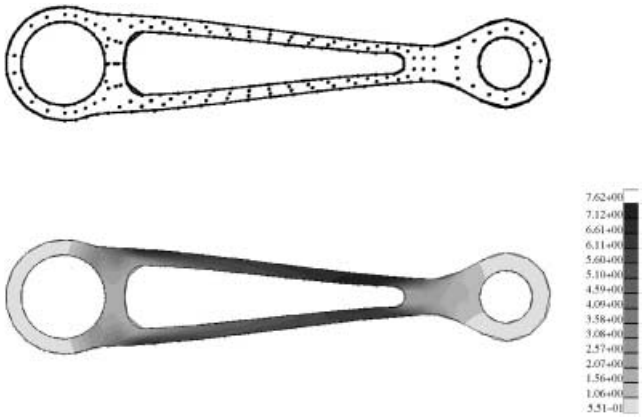

Fig. 5 Meshfree analysis result at optimum design after redistributing particles

4.2
Shape design optimization of a bracket

Figure 6 shows design parameterization, meshfree particle discretization, and response analysis results for a bracket problem. A total of 12 design parameters have been selected to change the inner/outer boundary of the bracket, while maintaining symmetry. A total of 276 meshfree particles (552 DOF) are distributed over the domain.

Figure 7 plots the stress sensitivity with respect to u_{12}. As design parameter u_{12} increases in value, the stress in the upper region of the inner space significantly increases. However, u_{12} also reduces the structure's mass. A trade–off analysis must be performed by the design en-

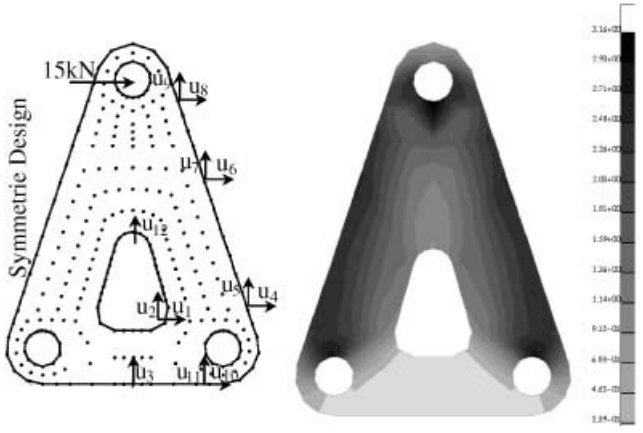

Fig. 6 Design parameterization and meshfree analysis result of bracket

gineer in order to select an appropriate amount of design perturbation in a manual design procedure.

The same design optimization problem defined in (59) has also been formulated to minimize the structural area or mass with respect to the stress constraints. The optimization problem converged in 17 iterations. Figure 8 shows the analysis results at the optimum design. The first eight iterations are used to reduce the structure's outer profile, with the inner triangle subsequently increasing in size until stress constraints have been activated. Because boundary conditions are given at the two side holes in the lower region of the bracket, the lower frame does not carry any load, and optimum results suggest that it can be removed. Since the existing domain cannot be removed during the shape optimization process, the optimizer must move the design parameters, corresponding to the lower frame, to the upper/lower bounds to reduce structural mass.

Optimal mass is reduced from 0.341 kg to 0.138 kg, which is 40.5% of the initial mass. The increased height of the inner triangle (u_{12}) produces the most significant reduction in structural mass, until stress constraints are activated at the side frame. The maximum value of stress (319 MPa), located at the top of inner triangle, moves to the side frame at 800 MPa. A total of 37 response analyses

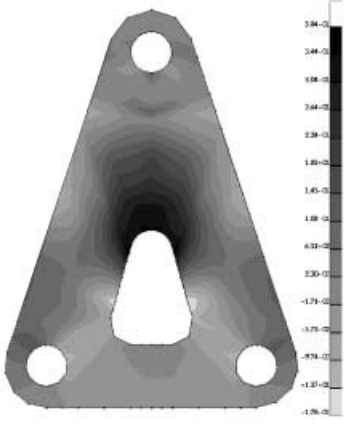

Fig. 7 Von Mises stress sensitivity with respect to u_{12}

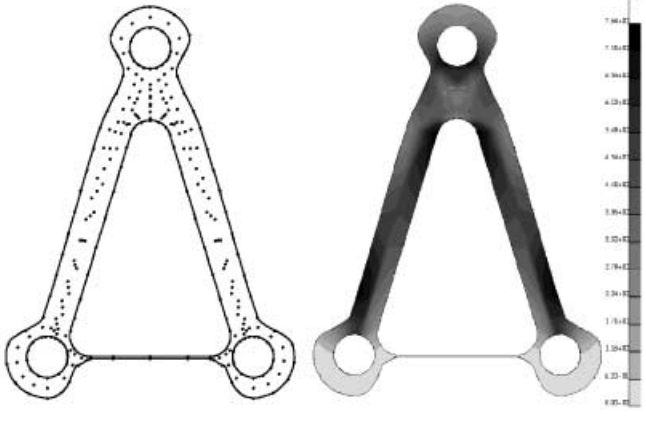

Fig. 8 Shape design optimization history

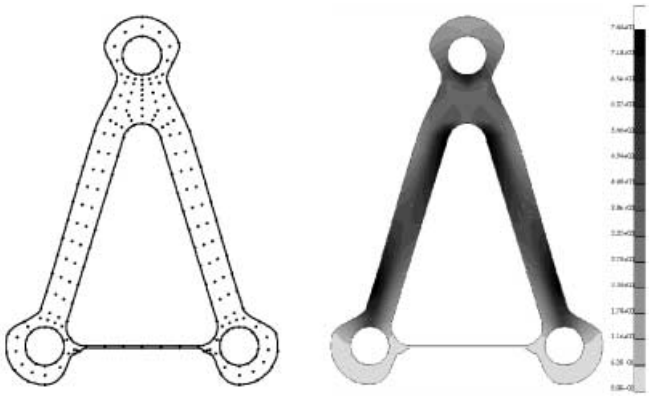

Fig. 9 Meshfree analysis result at optimum design with redistributed particles

and 17 DSA were carried out during 17 optimization iterations. When FEM is used with the re-meshing process (Bennett and Botkin 1985), the optimization process converges at 34 iterations with seven re-meshing processes. Thus, this approach reduces the cost of design about 50%, without factoring in the costs related to the re-meshing process.

Since the initial particle distribution is used throughout the design optimization process, particle distribution at the optimum design is very irregular, as shown in Fig. 8. To confirm the accuracy of analysis, remodelling is carried out to distribute particles evenly at the optimum design. Figure 9 shows that the analysis results using redistributed meshfree particles are very similar to the irregular distribution results in Fig. 8. Thus, it is again clear that particle distortion does not significantly detract from either solution accuracy or optimum results.

4.3 Shape design optimization of a road arm

The previous two examples use Gauss quadrature in the Galerkin meshfree method to integrate domain. For that purpose, a background mesh (integration zone) is still required, which is a drawback in the true sense of the meshfree method. Direct nodal integration, on the other hand, leads to numerical instability, due to an under integration and to derivatives of shape functions that vanish at the nodes. A strain-smoothing stabilization for nodal integration has been proposed by Chen *et al.* (2000b) to eliminate such spatial instability in nodal integration, and to provide the same level of accuracy as in Gauss quadrature. DSA for stabilized conforming nodal integration enhances computational efficiency and completely removes background mesh, so that the integration of the shape DSA and optimization can be effectively carried out.

In this section, a stabilized nodal integration method is employed to the design optimization of a 3-dimensional road arm, which transfers a force and torque from a road wheel to a suspension unit (see Fig. 10). Since the geome-

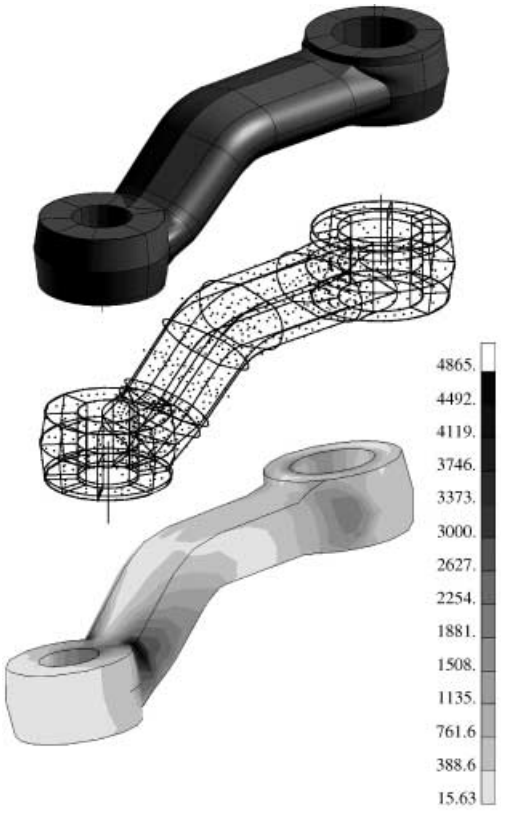

Fig. 10 Road arm model and meshfree analysis result

tries in the corner are so complicated, it is challenging to make a regular-shaped finite element. In addition to the complicated initial geometry, the structural shape further changes during design optimization process, which will cause a mesh distortion problem if a finite element method is used.

The road arm model is approximated by using 1455 meshfree particles (4365 DOF), without background mesh. The road arm is made of steel with $E = 206\,\text{GPa}$, and $\nu = 0.3$. At the center of the right hole, a vertical force of 3736 N and a torque of 44 516 Nm is applied, while the left hole is fixed. Unlike Gauss quadrature-based method in the previous two examples, the stress value is calculated at the particle position. As was illustrated in Fig. 10, the stress concentration appears in the left corner of the road arm. If the highest stress level in the left corner is considered as a reference value, then the dimension of the right corner cross-section can be reduced, because this region has a large safety margin.

Since two holes are connected to the road wheel and torsion bar, the dimension and the geometry of the holes are fixed. Thus, the design goal is to determine the dimension of the cross-sections of the arm. The heights and widths of four sections are selected as design parameters (see Fig. 11). Thus, a total of eight design parameters are considered in this example.

The design optimization is carried out to minimize the structural weight of the road arm, while maintaining the maximum stress level. Design optimization problem converges after eight iterations. Figure 12 compares the meshfree analysis result at the initial and optimum designs. The structural weight at the optimum design is reduced by 23% compared to the initial weight. Since the stress concentration appears in the left corner at the initial design, the optimization algorithm tried to reduce the cross–section of the right corner so that both parts may have the same level of stress values. Because of the significant geometry changes in the right corner, the mesh distortion problem may occur if the finite element-based analysis method is employed.

Through the three design optimization examples, it is concluded that the mesh distortion problem in the finite element-based shape design can be effectively resolved by using the meshfree method. In addition, it is shown that the solution accuracy of the meshfree method is insensitivity to the regularity of the particle distribution.

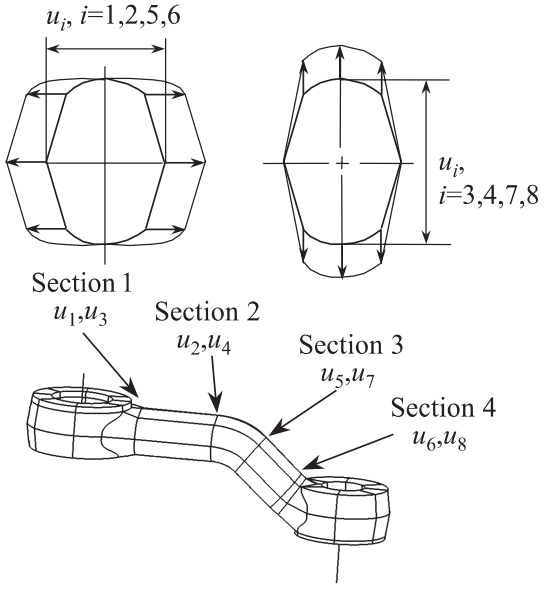

Fig. 11 Design parameterization of the road arm

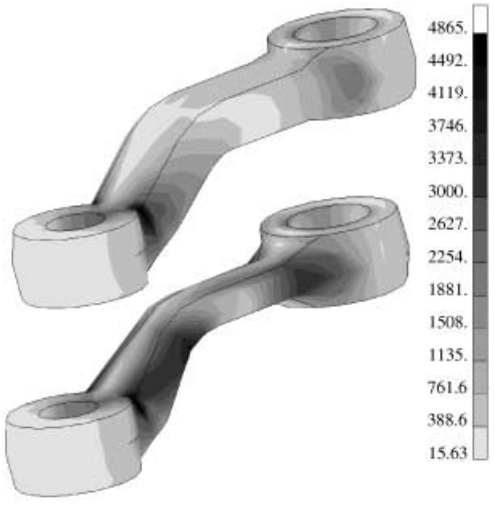

Fig. 12 Meshfree analysis result at the initial and optimum designs

5 Conclusions and plan

A numerical method of design sensitivity analysis and optimization using the meshfree method is proposed by discretizing continuum–based variational equations. Unlike finite element and boundary element methods, the shape function of the approximation depends on shape design parameterization, whose effects have been discussed in detail.

Shape design optimization of automotive parts undergoing large shape changes can be effectively carried out using meshfree methods that are insensitive to geometric distortions, without requiring re-meshing. Fast convergence of the design optimization algorithm is accomplished using the accurate sensitivity information. This approach reduces human interaction and design costs significantly during optimization, yet it maintains the same level of accuracy if not an even better level.

Acknowledgements This research is supported by General Motors and NSF/DARPA Optimized Portable Algorithms of Applications Libraries (OPAAL). This support is gratefully acknowledged.

References

Adelman, H.M.; Haftka, R.T. 1986: Sensitivity analysis of discrete structural systems. *AIAA J.* **24**, 823–832

Arora, J.S.; Cardoso, J.B. 1992: Variational principle for shape design sensitivity analysis. *AIAA J.* **30**, 538–547

Belegundu, A.D.; Rajan, S.D. 1988: A shape optimization approach based on natural design variables and shape functions. *Comp. Meth. Appl. Mech. Eng.* **66**, 87–106

Belytschko, T.; Lu, Y.Y.; Gu, L. 1994: Element free Galerkin method. *Int. J. Numer. Meth. Eng.* **37**, 229–256

Bennett, J.A.; Botkin, M.E. 1985: Structural shape optimization adaptive mesh refinement. *AIAA J.* **23**, 458–464

Chang, K.H.; Choi, K.K.; Tsai, C.S.; Chen, C.J.; Choi, B.S.; Yu, X. 1995: Design sensitivity analysis and optimization tool (DSO) for shape design applications. *Computing Systems in Engineering* **6**, 151–175

Chen, J.S.; Pan, C.; Wu, C.T.; Liu, W.K. 1996: Reproducing kernel particle methods for large deformation analysis of nonlinear structures. *Comp. Meth. Appl. Mech. Eng.* **139**, 195–227

Chen, J.S.; Wang, H.P. 2000a: New boundary condition treatments in meshfree computation of contact problems. *Comp. Meth. Appl. Mech. Eng.* **187**, 441–468

Chen, J.S.; Wu, C.T.; Yoon, S.; You, Y. 2000b: A stabilized conforming nodal integration for Galerkin meshfree methods. *Int. J. Numer. Meth. Eng.* **50**, 435–466

Choi, K.K.; Haug, E.J. 1983: Shape design sensitivity analysis of elastic structures. *J. Struct. Mech.* **11**, 231−269

Dems, K.; Mroz, Z. 1984: Variational approach by means of adjoint systems to structural optimization and sensitivity analysis, structural shape variation. *Int. J. Solids & Struct.* **20**, 527–552

Duarte, C.A.M.; Oden, J.T. 1996: A H–P adaptive method using clouds. *Comp. Meth. Appl. Mech. Eng.* **139**, 237–262

Grindeanu, I.; Chang, K.H.; Choi, K.K.; Chen, J.S. 1998: Design sensitivity analysis of hyperelastic structures using a meshless method. *AIAA J.* **36**, 618–627

Haber, R.B. 1987: A new variational approach to structural shape design sensitivity analysis. In: Mota Soares, C.A. (ed.) *Computer-aided optimal design*, pp. 573–587. Berlin, Heidelberg, New York: Springer

Kim, N.H.; Choi, K.K.; Chen, J.S.; Park Y.H. 2000a: Meshless shape design sensitivity analysis and optimization for contact problem with friction. *Comp. Mech.* **25**, 157–168

Kim, N.H.; Choi, K.K.; Chen, J.S. 2000b: Shape design sensitivity analysis and optimization of elasto-plasticity with frictional contact. *AIAA J.* **38**, 1742–1753

Kim, N.H.; Park, Y.H.; Choi, K.K. 2001: Optimization of a hyper-elastic structure with multibody contact using continuum–based shape design sensitivity analysis. *Struct. Multidisc. Optim.* **21**, 196–208

Lancaster, P; Salkauskas, K. 1981: Surface generated by moving least squares methods. *Math. Comp.* **37**, 141–158

Liu, W.K.; Jun, S.; Zhang, Y.F. 1995: Reproducing kernel particle methods. *Int. J. Numer. Meth. Fluids* **20**, 1081–1106

Melenk, J.M.; Babuska, I. 1996: The partition of unity finite element method: basic theory and applications. *Comp. Meth. Appl. Mech. Eng.* **139**, 289–314

The MacNeal–Schwendler Corp. 1999: *MSC/PATRAN user's guide.* Los Angeles, CA

Nayroles, B.; Touzot, G.; Villon, P. 1992: Generalizing the finite element method: diffuse approximation and diffuse elements. *Comp. Mech.* **10**, 307–318

Randles; P.W.; Libersky, L.D. 1996: Smoothed particle hydrodynamics: some recent improvements and applications. *Comp. Meth. Appl. Mech. Eng.* **139**, 375–408

Tortorelli, D.A.; Wang, Z. 1993: A systematic approach to shape sensitivity analysis. *Int. J. Solids & Struct.* **30**, 1181–1212

Vanderplaats, G.N. 1997: *DOT user's manual*. Colorado Springs, CO: VMA Corp.

Yao, T.M.; Choi, K.K. 1989: 3-D shape optimal design and automatic finite element regridding. *Int. J. Numer. Meth. Eng.* **28**, 369–384